

RESEARCH ARTICLE

Localization of an ultra wide band wireless endoscopy capsule inside the human body using received signal strength and centroid algorithm

Memduh Suveren, Rüştü Akay*, Muzaffer Kanaan

Department of Mechatronics Engineering, Erciyes University, Kayseri 38039, Turkey
msuveren@erciyes.edu.tr, akay@erciyes.edu.tr, mkanaan@erciyes.edu.tr

ARTICLE INFO

Article history:

Received: 20 August 2021

Accepted: 31 May 2022

Available Online: 26 July 2022

Keywords:

Centroid algorithm

Wireless capsule endoscopy

In-body localization

RSS based model

Body model

AMS Classification 2010:

65K10, 49M05

ABSTRACT

Wireless capsule endoscopy (WCE) is used for imaging and diagnosing diseases in the gastrointestinal (GI) system. The location of the disease detected by WCE is still an important problem. Location information is very important for the surgical or drug treatment of the detected disease. In this study, RSS-based centroid algorithm has been used in order to accurately predict the capsule position on a sample data set. The effect of different parameters such as number of sensors used on the proposed mathematical model, location of sensors on positioning is analyzed in detail. The results show that a precise position detection is possible with fewer sensors positioned correctly. As a result, the positioning error with the correctly selected sensors is reduced by approximately 55%. In addition, the performance of the proposed method was compared with the classical centroid algorithm and more than 50% improvement was achieved.



1. Introduction

Wireless capsule endoscopy (WCE) is fast becoming an important technique in modern medical imaging, allowing parts of the human body (such as the small intestine) that could not be effectively imaged using conventional techniques [1]. WCE allows the diagnosis of illnesses such as colorectal cancer, celiac disease, Crohn's disease, the sites of intestinal bleeding and other types of pathologies in the gastrointestinal (GI) tract [2, 3]. A very attractive characteristic of WCE is that, unlike conventional endoscopy techniques, it causes little to no discomfort for the patient; the patient simply has to swallow a pill-shaped camera (i.e. the endoscopy capsule), which contains all the electronics for imaging and transmission of the image data to an on-body recording unit (see Figure 1 for the general system structure). The pill-shaped camera naturally moves through the GI tract and is naturally excreted out of the body. The images captured by the capsule are sent via an on-board radio transmitter to on-body receiving antennas and from there to a recording system. The images can then be reviewed offline by a medical specialist. Although the current generation of WCE systems use the medical implant communications system (MICS) band, there are proposals calling for the use of Ultra Wide Band (UWB) technology as well [4].

The primary advantage of UWB is the low power consumption due to simple transceiver structures required [5, 6]. In another type of WCE, camera is replaced with sensors such as temperature, pressure, Potential of Hydrogen or light spectrum analyser sensors [7, 8]. WCE could locate the abnormalities in GI system. Image processing algorithms detect diseases and notify the doctors [9]. Also, some works have focused on other external localization techniques based on magnetic field [10, 11].

Current WCE systems have a significant problem in the sense that there is no way to localize the capsule as it moves through the GI tract [12]. This means that if any of the images reveal a potentially abnormal condition (such as a tumor or a lesion) there is no way to know just where in the GI tract the condition exists, making subsequent surgical interventions very difficult and more risky for the patient [13]. Thus, it is critical to come up with techniques to accurately localize the endoscopy capsule as it moves through the GI tract. Localization of a source emitting a radio frequency (RF) signal on the basis of received signal characteristics is a well-investigated topic that has received much attention in the literature [14, 15]. One example of received signal characteristics that can be used for localization purposes is the received signal

*Corresponding author

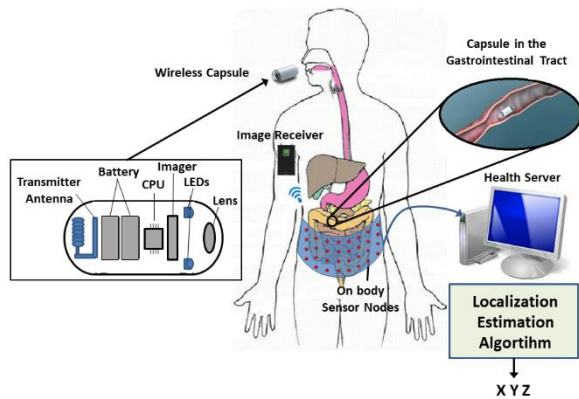


Figure 1. General system structure

strength (RSS). The usage of the RSS for localization purposes is attractive, as RSS is a very simple parameter to measure. This is why RSS has been preferred for challenging applications such as indoor localization [16]. For the in-body localization of an endoscopy capsule, however, RSS-based localization can be challenging. The in-body environment is highly non-homogeneous, consisting of different types of tissue, whose electrical conductivity and permittivity are frequency-dependent. For example, tissues such as skin, muscle, kidney, liver may have higher dielectric constant and conductivity (since these tissues contain a high amount of water), while dielectric constant and conductivity in tissues such as fat and bone with less water content may be lower. It is important to note that these parameters are also dependent on frequency [17]. This non-homogeneous environment can seriously distort UWB signals as documented by several prior studies in this area [18, 19, 20]. One way to combat these detrimental effects and obtain consistent accuracy in localization is to use more sensors (more receiving antennas) distributed over the body surface. This can provide performance gains, in a similar fashion to the diversity concept commonly used in other types of wireless communication systems [21, 22].

To explain this concept more clearly, consider the scenario of Figure 1, where the patient swallows the capsule and the signal emitted by the capsule is sensed by N antennas distributed over the body surface. Because of the inhomogeneity in the body environment, not all of these N antennas will be able to provide RSS measurements at the same quality; some will be of higher quality than others. The basic idea is to combine the measurements in such a way that higher-quality measurements have more impact on the final location estimate, while the lower-quality measurements are de-emphasized or excluded from the final location estimate altogether. There are two key questions that need to be answered in this context. First, considering the inhomogeneous nature of the in-body environment, which and how many of these N sensors should be used? Second, how should the measurements be combined to give an accurate location estimate? In this paper, we address these questions. To address the first question, we present a systematic analysis of

which sensors have the greatest contribution to a high-accuracy location estimate. To the best of our knowledge, this paper represents the first time in open literature that such a systematic analysis has been undertaken. For the second question, we propose a nonlinear analytical model for the RSS measurements, which can be used to estimate the location of the capsule. An analysis of the localization accuracy for the proposed model is also given, on the basis of a computerized 3-D body model. In this study, centroid algorithm was used to calculate the location of the capsule from the RSS measurement data on the human body model. Although the centroid algorithm was used mostly for indoor and WSN positioning operations [23, 24], we used this algorithm for in-body localization.

The rest of this paper is organized as follows. Section 2 gives details of the simulation environment which is used for performance evaluation and details the proposed nonlinear RSS model. Results are presented in Section 3. Section 4 concludes the paper.

2. Methods and procedures

2.1. The simulation environment

In order to evaluate positioning performance within the body, a 3-D voxel model of the human body is required first. For this purpose, 3-D human model obtained from Visible Human Project is used [25]. The 3-D human body model adopted for this study came integrated into the analysis software. This model contains the location of all tissues in the human body as well as all electromagnetic properties of all tissues such as dielectric permittivity and conductivity. Since this study focused on the small intestine region, the organs such as the head, arm and leg were not included in the model in order to reduce simulation time. Figure 2 shows the 3-D voxel model of the whole body and the truncated body model to reduce the simulation time, respectively. To analyze the behavior of the electromagnetic signals in the voxel model, XFDTDTM software from Remcom Inc. was used. This software uses Finite Difference Time Domain (FDTD) techniques to numerically solve Maxwell equations and obtain the electric and magnetic field intensities in the working area by considering material properties and boundary conditions.

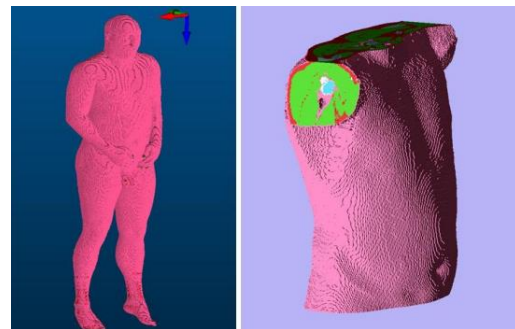


Figure 2. The whole-body model and the truncated body model used at simulations

In order to solve Maxwell's equations numerically, the body model is divided into small parts, or cells. The size of these cells, or cell size, must be calculated based on the smallest wavelength value of the signal.

This constraint, called the Courant limit, is "10 cells per wavelength", meaning that the side of each cell should be $\lambda/10$ or less at the highest frequency (shortest wavelength) of interest [18, 26]. In accordance with the Courant limit, the FDTD cell size used in the simulation was set to 1.2 mm in the x, y and z directions. The Perfectly Matched Layer (PML) boundary condition with 7 absorbing layers was also applied to prevent the reflection of the signals to the body environment. After defining the body model, the elliptic dipole type UWB antenna was placed in the simulation model. This antenna, which measures 20x12x4 mm, consists of two elliptical conductors and a dielectric case that isolates it from the body tissues [27]. A modulated gaussian pulse with center frequency of 4.1 GHz and -10 dB band width of 1.4 GHz was applied to the gap between two ellipses of the antenna. Also, the antenna input impedance was set to 50 ohm and the input power was fixed at 1mW. This applied signal satisfies to the frequency between 3.1 GHz and 4.8 GHz that known as "UWB Low Band" [28]. This band is in a range where signal attenuation is less when compared to the entire UWB band.

In the simulations, the antenna was placed in 64 different positions in the small intestine characterize the electric and magnetic field intensities within this region, as shown in Figure 3. The data for 48 of these 64 antenna position was used to optimize the parameter set for the localization algorithm and the remaining 16 positions were used to test the performance of the algorithm. In Figure 3, red and green antenna positions indicate the training and testing localizations, respectively.

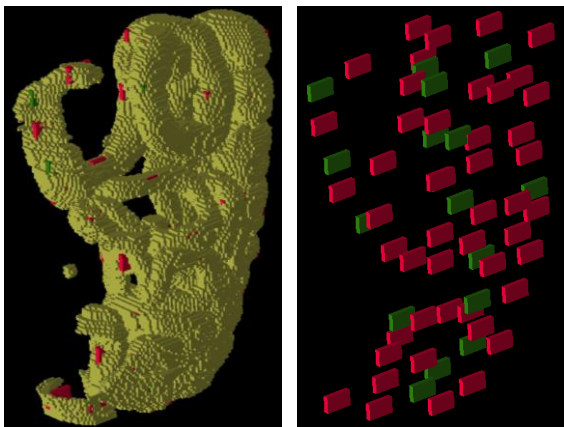


Figure 3. Small intestine in the model, test and train positions of the antenna

In order to determine the position of the wireless capsule within the small intestine, 256 point sensors are defined in the software on the body surface to observe the electric and magnetic field intensity. In telecommunications, particularly in radio, signal

strength refers to the magnitude of the electric field at a reference point that is at a significant distance from the transmitting antenna. This structure, defined as a point sensor in the program, represents small-size sensors that measure the amplitude and strength of electromagnetic signals in the time domain. As shown in Figure 4, each point sensor is on the body surface and sensors are arranged in 8 rows. The sensors were distributed around the body with 48 sensors on the front side, 80 on the back, 48 on the right side and 48 on the left.

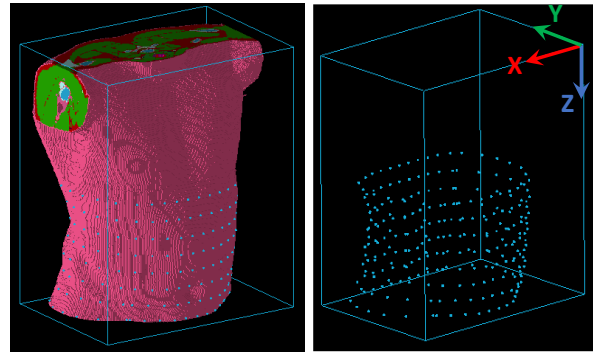


Figure 4. Sensor placement on the body model

Sensors placed on the body were used to calculate the Poynting vector. The Poynting vector, which is the vector cross product of the electric field and magnetic field intensity, is defined as,

$$\mathbf{P}(t) = \mathbf{E}(t) \times \mathbf{H}(t) \tag{1}$$

where $\mathbf{E}(t)$ and $\mathbf{H}(t)$ are the electric and magnetic intensities respectively and both are time dependent. The Poynting vector measured from each sensor gives the power density per unit area (W/m^2). 256 Poynting vectors were calculated in each of the 64 different transmitting antenna positions in the small intestine which resulted $64 \times 256 = 16,384$ data sets. The integral of the Poynting vector results in signal energy density (J/m^2) given as,

$$e = \int_t |\mathbf{P}(t)| dt \tag{2}$$

The energy density values obtained from the sensors were used to determine the position of the wireless capsule in the small intestine. Thus, the antenna position estimation was performed using a RSS-based mathematical model determined in the next section.

2.2. RSS-based in body localization using the centroid algorithm

In RSS-based positioning, energy values measured by the sensors placed on the body and the location of the sensors are used to obtain the localization of the capsule. The centroid algorithm used in positioning calculation has some similarities to the calculation of the center of the gravity for an object [29]. In this model, the energy intensity value measured by all sensors is associated with their location and the energy intensity center is calculated. Later, the position of this

center point is determined as the position of the transmitter capsule antenna. In order to derive the RSS based mathematical model, the following template was proposed.

$$\begin{aligned}\hat{X}_k &= \sum_{i=1}^N \frac{X_{S_i} (E_i)^{\alpha_x}}{\left(\sum_{j=1}^N (E_j)^{\alpha_x} \right)}, \\ \hat{Y}_k &= \sum_{i=1}^N \frac{Y_{S_i} (E_i)^{\alpha_y}}{\left(\sum_{j=1}^N (E_j)^{\alpha_y} \right)}, \\ \hat{Z}_k &= \sum_{i=1}^N \frac{Z_{S_i} (E_i)^{\alpha_z}}{\left(\sum_{j=1}^N (E_j)^{\alpha_z} \right)}\end{aligned}\quad (3)$$

where $(\hat{X}_k, \hat{Y}_k, \hat{Z}_k)$ are the estimated coordinates of k -th transmitting antenna in the small intestine, $(X_{S_i}, Y_{S_i}, Z_{S_i})$ are the coordinates of i -th sensor on the body, E_i is energy density which computed at Eq. (2) for i -th sensor. Also $\alpha = [\alpha_x, \alpha_y, \alpha_z]$ is defined as exponent that gives nonlinearity for all coordinates and N is the total number of sensors with the highest energy used at model. With this model, the position of the antennas in the intestine were estimated by the known positions of the sensors and the energy density values obtained from these sensors.

The energy density values obtained from the point sensors were arranged in order of magnitude for effective localization for each transmit antenna position. Then N sensors with the highest energy density values were selected from the sorted data set. Thus, in the estimation of the antenna position, the effect of sensors with higher energy density values were higher, while those with lower energy density were ignored. In addition, the vector of exponents α , which model the nonlinear effects of the human body environment on energy density [19], increases the sensitivity of the RSS-based model. There are different types of tissues in the body and the behavior of each one is frequency dependent. This makes the human body extremely nonlinear from the perspective of electromagnetic wave propagation [19]. For this reason, nonlinearity parameter was added to the proposed model and the results were examined. In the next section, the effect of α on positioning accuracy is examined in more detail. The performance of the localization model was evaluated together with range estimation errors. The localization error can be calculated using the following equation:

$$\varepsilon_k = \sqrt{(X_k - \hat{X}_k)^2 + (Y_k - \hat{Y}_k)^2 + (Z_k - \hat{Z}_k)^2} \quad (4)$$

where (X_k, Y_k, Z_k) is the real antenna location and ε_k

is the localization error of k -th antenna location.

3. Results

The results obtained in this article are examined under three main headings. For the best performance, the results for the number of sensors, sensor topology and α parameters are examined. Firstly, how many of the 256 point sensors placed on the body will be used in the positioning calculation is determined. Then, effect of the sensors distributed around the body on the positioning accuracy is examined according to the body region where the sensor is located. Finally, the effect of parameter α , described in the previous section, on positioning accuracy was examined. These 3 topics are discussed in detail in this section.

3.1. Effect of the number of sensors

As mentioned in the previous sections, energy values were obtained from 256 point sensors placed on the body surface. At this point, how many of these sensors should be included in the algorithm? In order to find the answer to this question, firstly, the effect of N used in the Eq. (3) on the localization error were investigated. While examining the effect of the number of sensors, α was kept constant [1,1,1]. Considering α to be constant is only for the purposes of investigating the effect of the number of sensors (N) on localization. The relationship between the number of sensor (N) and localization error is presented in Figure 5. Here, the effect of using a variable number of sensors for 64 different capsule positions is examined and the RMS value of 64 capsule localization errors for each N value is calculated by Eq. (4).

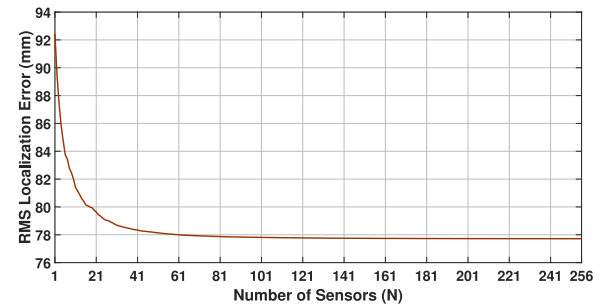


Figure 5. The relationship between number of point sensors (N) and localization error

From Figure 5, it is clearly seen that using a large number of sensors (N) does not affect the positioning error after a certain point. There is a 2.6% difference between using 20 sensors and 256 sensors in the model. Therefore, $N=20$ was selected in the following sections to reduce the complexity of the model. On the other hand, another important issue is that the X, Y and Z errors are different in the antenna position estimation. The next question is: what is the reason for these high localization errors? To answer this question coordinate estimation errors are calculated separately and plotted in Figure 6.

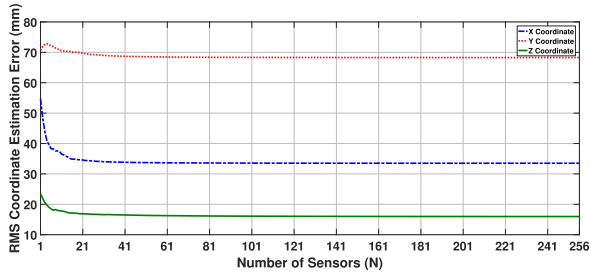


Figure 6. The relationship between number of point sensors (N) and coordinate estimation errors

As seen in Figure 6, the highest contribution to the localization error is from the Y coordinate estimate. When N parameter set to 20, the total localization error is 79.77 mm while the X, Y and Z antenna position estimation errors are 34.62 mm, 69.85 mm and 16.89 mm respectively. To improve these results, we have noticed that it is not sufficient to just change the number of sensors, and therefore different processes will be performed for estimating each coordinate of the capsule in the following sections.

3.2. Effect of the selected sensor region

As the localization error was very high in the previous section, we tried to reduce this error with new approaches. In order to determine the location of the capsule in the intestine, the region of the sensors were also taken into account. In other words, the effect of sensors located in different parts of the body on positioning performance has been examined. 4 different regions were examined for 256 sensors distributed around the body. As mentioned in Section 2.1, sensors were distributed around the body with 80 sensors on the front side, 80 on the back, 48 on the right side and 48 on the left as shown in Figure 7.

In this scenario, the objective is to select 20 sensors to be used in positioning calculation only from the specified body regions, not from all sensors around the body. The sensors to be included in the positioning calculation in the relevant regions are selected according to the energy density values. Thus, 20 sensors reporting the highest energy density values are included in the calculation each time. As a result, location estimation is made for 64 different capsule

locations and the RMS localization errors obtained are shown in Table 1.

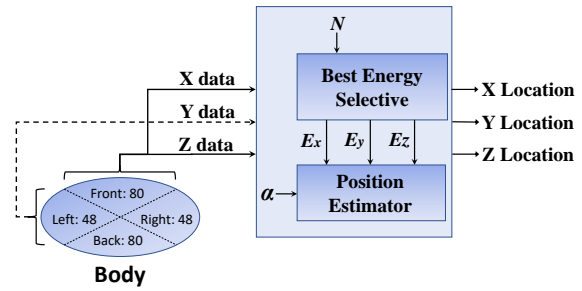


Figure 7. The final localization flow diagram

The results of Table 1 indicate that the body region on which the sensors are placed has a great influence on the positioning error. The bold marked values in the table represent the lowest errors obtained in the relevant coordinate. When the 80 sensors in front of the body are used, the X position error is 15.45 mm and the Z position error is 16.24 mm, which means a 55.4% and 3.8% improvement respectively compared to results presented in Figure 6. Also in case of the 48 sensors on the left side of the body being used, the Y position error is 28.14 mm and this provides a 59.7% improvement. According to the coordinate system given in Figure 4, the Y coordinate gives the depth information towards the inside of the body and the positioning error is higher compared to the X and Z coordinates. This is because the body is not homogeneous, and the sensor spacing and number are not the same in the lateral and anterior planes. On the other hand, it is seen that the Right-side sensors have a negative effect on the calculation of the X position and the Back sensors on the Y, Z positions. As a result, some sensors provide the better results for some coordinates, while they may have a negative impact on the other coordinates. Therefore, using all sensors together doesn't make any sense for localization estimate. The data taken from the sensors which are based on the RSS-based measurement were subjected to a flow diagram as in Figure 7.

The main takeaways from these results so far are as follows. First, it does not make sense to just use all the sensors distributed on the body surface, as they do not all provide measurements at the same quality.

Table 1. Effect of the selected sensor region on the positioning error

Sensor Location	RMS Coordinate Estimation Error			RMS Localization Error (mm)
	X (mm)	Y (mm)	Z (mm)	
Front	15,45	85,75	16,24	88,63
Left Side	126,90	28,14	49,17	138,98
Back	39,50	190,87	78,37	210,08
Right Side	187,02	35,34	59,63	199,45
Front + Left Side	35,34	72,71	16,30	82,47
Front + Right Side	19,24	83,47	16,77	87,29
Front + Back	16,19	79,87	16,93	83,24
Left Side + Right Side	85,31	28,97	36,66	97,27
All	34,62	69,85	16,89	79,77

The use of a more limited subset (selected in accordance with the flow diagram of Figure 7) will result in more accurate estimates of the capsule location. Furthermore, it is possible to accomplish this accuracy improvement at a lower overall system cost, as less on-body sensors will now need to be used. Having said that, it is possible to improve the accuracy even further by making adjustments on how the energy readings from the various sensors are incorporated into the final location estimate, as will become clear from the results of the next section.

3.3. The effect of the α parameter

All the data so far has been obtained for $\alpha_x = \alpha_y = \alpha_z = 1$. As previously mentioned, α provides a nonlinear characteristic for the mathematical model. Setting the α parameter to 0 means ignoring the effect of the energy density at the mathematical model. Similarly, making the α parameter 1 means that the energy density will provide a linear effect, making it >1 shows energy density more effective and making it <1 energy density less effective.

Some of the antenna locations to examine the effect of this parameter on the positioning error have been reserved to test the performance of algorithm. As a result, antenna locations have been decomposed for 16 and 48 antennas, as previously described in Section 2.1. Thus, the 16 antenna positions have been used to test the performance of the algorithm and remaining were used to derive the α parameters. For each alpha value, RMS value of error data obtained in 16 different capsule test positions was calculated. The test positions of the capsule were previously shown in Figure 3 (green positions). Figure 8 shows the effect of the parameter α on the individual positioning error for X, Y and Z.

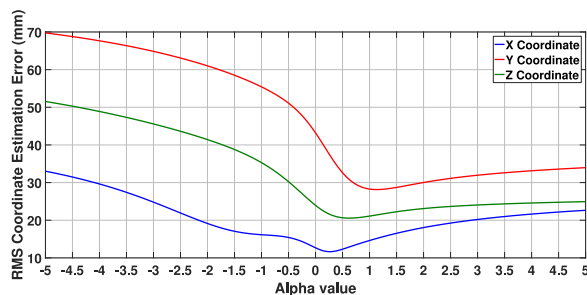


Figure 8. Alpha (α) parameter effect on the coordinate estimation errors for test points

At the Figure 8, it was tried to optimize the value of α between -5 and 5 for the test antenna locations and optimum results were obtained as $\alpha_x = 0.42$, $\alpha_y = 1.20$, $\alpha_z = 0.64$ values. In addition, when the graph was examined in a wider range between -100 and 100, it was seen that the error remained constant at very low or very large values of α .

In order to achieve the final improvement rate, these α

values were used at the test locations as shown in Table 2. As a result, the RMS localization errors obtained for the number of $N=20$ sensors (explained in Section 3.1), the sensors selected from the body regions shown in Figure 7 (explained in Section 3.2) and the calculated optimum α values are given in Table 2.

Table 2. Effect of the ideal α parameters on the positioning error ($\alpha_1 = [1,1,1]$ and $\alpha_2 = [0.42, 1.2, 0.64]$)

Data Type	RMS(mm)		%
	α_1	α_2	
Train Antenna Loc	35,21	33,15	5,85
Test Antenna Loc.	38,19	36,88	3,43
All Antenna Loc.	35,98	34,12	5,17

From the Table 2, we can obviously find that the inclusion of 3 different alpha parameters in the mathematical model, improvement of 5.85% and 3.43% was obtained for the training and testing antenna locations, respectively. Consequently, maximum RMSE localization error of 36,88 mm has been achieved.

For a different perspective on these results, we can infer from Table 1 in Section 3.2 that, the localization error using all sensors is the 79.77mm. On the other hand, in the case of using Left-side sensors for Y data and Front sensors for X and Z data, the localization error falls to 35.98 mm for all antenna locations. Here, it is clear that a 54.9% improvement in position error of wireless capsule was achieved. Thus, it can be said that the total improvement is 57.2% by including the results obtained in Section 2.2 into the mathematical model.

3.4. Comparison of the proposed algorithm with the classical centroid algorithm

Although the centroid algorithm is frequently used in indoor positioning and WSN (Wireless Sensor Network) scenarios, it is not widely used in in-body localization. It may be instructive to compare the results to other UWB-based localization of the endoscopic capsule in the small intestine operating for the in-body context. Unfortunately, in the course of our literature search, we were unable to find any other works except [30] dealing with UWB-based in-body localization through centroid algorithm that would allow a direct comparison. In the [30], the path loss model was used together with the centroid algorithm for positioning, but the effects of body tissues and sensor topology on positioning were not studied. In this respect, our study fills the gap in the literature in terms of both using a realistic human model and providing capsule positioning using the RSS data directly in the centroid algorithm. For these reasons, we compared the proposed centroid algorithm with the classical centroid algorithm used in indoor positioning and examined its performance.

The classical centroid algorithm used in [31, 32] studies

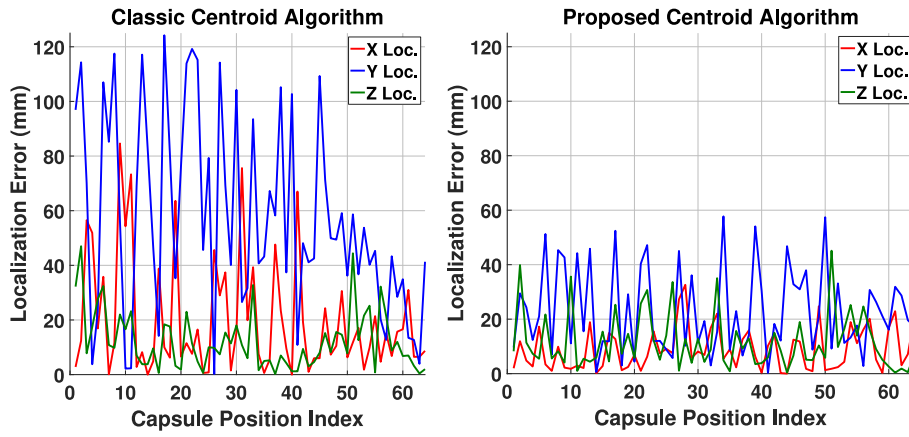


Figure 9. Localization errors of classical and proposed algorithms

is given as in Eq. 5.

$$\hat{X}_k = \sum_{i=1}^N \frac{X_{S_i}}{N}, \hat{Y}_k = \sum_{i=1}^N \frac{Y_{S_i}}{N}, \hat{Z}_k = \sum_{i=1}^N \frac{Z_{S_i}}{N} \quad (5)$$

where N is sensor number, $(\hat{X}_k, \hat{Y}_k, \hat{Z}_k)$ are the estimated coordinates of k -th transmitting antenna, $(X_{S_i}, Y_{S_i}, Z_{S_i})$ are the coordinates of i -th sensor. This equation basically calculates the average of the positions of N sensors with the best energy value. While comparing the performance with the classical centroid algorithm, the energy density values of 256 sensors around the body were measured for each capsule position, and the positions of the 20 sensors with the strongest energy density were used. As a result, the RMS positioning errors of the proposed centroid algorithm and the classical centroid algorithm for 64 capsule positions are shown in Figure 9. As can be seen in the Figure 9, errors are higher in the classical centroid algorithm. In terms of RMS values of X, Y, and Z localization error, the error values of the proposed centroid algorithm are 59.5%, 58.8% and 3.9% less than classic centroid algorithm, respectively. In another comparison, the cumulative probability function of the distance estimation errors was obtained as in Figure 10.

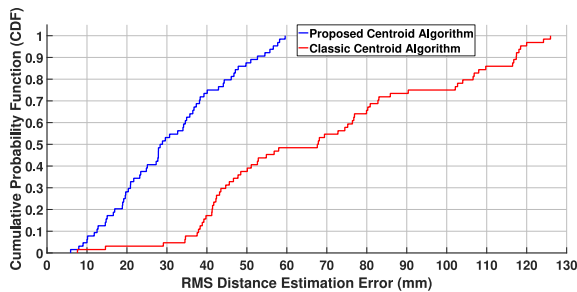


Figure 10. Comparative CDF values of localization errors

When Figure 10 is examined, the distance estimation error of the classical centroid algorithm is much higher, for example, the distance estimation error with 80%

probability is below 44mm for the proposed centroid algorithm, while the error in the classical algorithm is below 104mm under the same conditions.

We end this section with comments as to how the techniques outlined in this paper can be applied in practice. If this technique is used in real life, it is possible to localize the capsule that moves within the intestine with a low error with the sensor set physically placed on the body and the simple centroid algorithm. The proposed Centroid algorithm implementation is simple, has low computational load and provides positioning with only energy density measurements. The disadvantage of this algorithm is that if the sensor positions are measured incorrectly, the positioning performance will be greatly reduced.

4. Conclusion

In this paper, we have presented a detailed study on a new RSS-based mathematical model applicable for UWB-based wireless capsule localization in the small intestine. Relationships for the mathematical model parameters, namely the N sensor number, the exponent α and the energy density have been presented. We have used the proposed mathematical model to determine the optimal location and number of the received signal sensors to improve localization accuracy. The results indicate that usage of a large number of sensors distributed all over the body surface has no beneficial impact on positioning accuracy, as all the sensors will not provide measurements at the same quality. Opportunistic deployment of a lesser number of sensors in certain parts of the body (such as the front and left sides of the torso), are seen to result in a reduction of the overall localization error, and will no doubt reduce the overall system-cost. In addition, the performance of the proposed method was compared with the classical centroid algorithm and more than 50% improvement was achieved. These results shed light on precise, cost-effective positioning of the wireless endoscopy capsule in the gastrointestinal tract with a simple RSS technique in the future.

Acknowledgment

The authors would like to acknowledge and thank the Scientific Research Projects Support Office of the Erciyes University, which has supported this work under grant number FDK-2018-7833.

References

- [1] Mateen, H., Basar, R., Ahmed, A. U., & Ahmad, M. Y. (2017). Localization of wireless capsule endoscope: A systematic review. *IEEE Sensors Journal*, 17(5), 1197-1206.
- [2] Kumar, R., Zhao, Q., Seshamani, S., Mullin, G., Hager, G., & Dassopoulos, T. (2012). Assessment of crohn's disease lesions in wireless capsule endoscopy images. *IEEE Transactions on Biomedical Engineering*, 59(2), 355-362.
- [3] Woods, S.P., & Constandinou, T.G. (2013). Wireless capsule endoscope for targeted drug delivery: Mechanics and design considerations. *IEEE Transactions on Biomedical Engineering* 60(4), 945-953.
- [4] Davenport, D., Hernandez, M., Lewis, D., Li, H. B., McPartland, R., Omeni, O., & Astrin, A. (2011). IEEE 802.15. 6 Tutorial. *IEEE P802*, 15.
- [5] Yuce, M.R., Keong, H.C., & Chae, M.S. (2009). Wideband communication for implantable and wearable systems. *IEEE transactions on microwave theory and techniques* 57(10), 2597-2604.
- [6] Khaleghi, A., Chavez-Santiago, R., & Balasingham, I. (2010). Ultra-wideband pulse-based data communications for medical implants. *IET communications* 4(15), 1889-1897.
- [7] Alam, M. W., Vedaiei, S. S., & Wahid, K. A. (2020). A fluorescence-based wireless capsule endoscopy system for detecting colorectal cancer. *Cancers*, 12(4), 890.
- [8] Khan, A. H., Sohag, M. H. A., Vedaiei, S. S., Mohebbian, M. R., & Wahid, K. A. (2020). Automatic detection of intestinal bleeding using an optical sensor for wireless capsule endoscopy. In *2020 42nd Annual International Conference of the IEEE Engineering in Medicine & Biology Society (EMBC)* (pp. 4345-4348). IEEE.
- [9] Deeba, F., Bui, F. M., & Wahid, K. A. (2020). Computer-aided polyp detection based on image enhancement and saliency-based selection. *Biomedical signal processing and control*, 55, 101530.
- [10] Wang, M., Shi, Q., Song, S., Hu, C., & Meng, M. Q. H. (2019). A novel relative position estimation method for capsule robot moving in gastrointestinal tract. *Sensors*, 19(12), 2746.
- [11] Shao, G., Tang, Y., Tang, L., Dai, Q. & Guo, Y. (2019). A Novel Passive Magnetic Localization Wearable System for Wireless Capsule Endoscopy, *IEEE Sensors Journal*, 19(9), 3462-3472.
- [12] Than, T.D., Alici, G., Zhou, & H., Li, W. (2012). A review of localization systems for robotic endoscopic capsules. *IEEE Transactions on Biomedical Engineering* 59(9), 2387-2399 .
- [13] Pahlavan, K., Geng, Y., Cave, D. R., Bao, G., Mi, L., Agu, E., ... & Tarokh, V. (2015). A novel cyber physical system for 3-D imaging of the small intestine in vivo. *IEEE Access*, 3, 2730-2742.
- [14] Wang, Y., Fu, R., Ye, Y., Khan, U., & Pahlavan, K. (2011, January). Performance bounds for RF positioning of endoscopy camera capsules. In *2011 IEEE Topical Conference on Biomedical Wireless Technologies, Networks, and Sensing Systems*, 71-74.
- [15] Mao, G., Fidan, B., & Anderson, B.D. (2007). Wireless sensor network localization techniques. *Computer networks* 51(10), 2529-2553.
- [16] Achroufene, A., Amirat, Y., & Chibani, A. (2018). RSS-based indoor localization using belief function theory. *IEEE Transactions on Automation Science and Engineering*, 16(3), 1163-1180.
- [17] Gabriel, C., Gabriel, S., & Corthout, Y. E. (1996). The dielectric properties of biological tissues: I. Literature survey. *Physics in medicine & biology*, 41(11), 2231.
- [18] Suveren, M. (2015). *Ultra wide band (uwb) wireless systems in implant body area networks and modelling of the distance measurement error*. MSc Master thesis, Erciyes University, Kayseri.
- [19] Kanaan, M., & Suveren, M. (2015). A novel frequency-dependent path loss model for ultra wideband implant body area networks. *Measurement* 68, 117-127.
- [20] Kanaan, M., & Suveren, M. (2017). In-body ranging with ultra-wideband signals: Techniques and modeling of the ranging error. *Wireless Communications and Mobile Computing*, 2017.
- [21] He, F., Man, H., & Wang, W. (2011). Maximal ratio diversity combining enhanced security. *IEEE Communications Letters* 15(5), 509-511.
- [22] Alamouti, S. M. (1998). A simple transmit diversity technique for wireless communications. *IEEE Journal on selected areas in communications*, 16(8), 1451-1458.
- [23] Liu, Y., Jin, M., & Cui, C. (2010). Modified weighted centroid localization algorithm based on rssi for wsn. *Chinese Journal of Sensors and Actuators* 23(5), 717-721
- [24] Pivato, P., Palopoli, L., & Petri, D. (2011). Accuracy of rss-based centroid localization algorithms in an indoor environment. *IEEE Transactions on Instrumentation and Measurement* 60(10), 3451-3460.
- [25] Ackerman, M. J., Spitzer, V. M., Scherzinger, A. L., & Whitlock, D. G. (1995). The Visible Human data set: an image resource for anatomical visualization. *Medinfo* 8, 1195-1198.

- [26] Kunz, K. S., & Luebbers, R. J. (1993). *The finite difference time domain method for electromagnetics*. CRC press.
- [27] Khaleghi, A., & Balasingham, I. (2009). Improving in-body ultra wideband communication using near-field coupling of the implanted antenna. *Microwave and Optical Technology Letters* 51(3), 585-589.
- [28] Wang, Q., Masami, K., & Wang, J. (2009, September). Channel modeling and BER performance for wearable and implant UWB body area links on chest. In *2009 IEEE International Conference on Ultra-Wideband* (316-320).
- [29] Kaiser, M.J., & Morin, T.L. (1993). Algorithms for computing centroids. *Computers and operations research*, 20(2), 151-165.
- [30] Hany, U., Akter, L., & Hossain, F. (2017). Degree-based wcl for video endoscopic capsule localization. *IEEE Sensors Journal*, 17(9), 2904-2916.
- [31] Bulusu, N., Heidemann, J., & Estrin, D. (2000). GPS-less low-cost outdoor localization for very small devices. *IEEE personal communications*, 7(5), 28-34.
- [32] Kaur, A., Kumar, P., & Gupta, G. P. (2019). A weighted centroid localization algorithm for randomly deployed wireless sensor networks. *Journal of King Saud University-Computer and Information Sciences*, 31(1), 82-91.

Memduh Suveren received his M.S degree in *Mechatronics Engineering* from Erciyes University in 2015. He has been working as a research assistant in *Mechatronics Engineering* department since 2011,

Erciyes University. His current research interests include *Wireless Capsule Endoscopy, Ultra-Wide Band (UWB) signaling, in body localization, Magnetic Capsule localization and Electromagnetic studies*.

 <http://orcid.org/0000-0003-4545-5378>

Rüştü Akay received the M.S. and the Ph.D. degree in *computer engineering* from Erciyes University, Kayseri, Turkey, in 2006 and 2014, respectively. Since 2014 he is an Assistant Professor in the Department of *Mechatronics Engineering*, Erciyes University. His current research interests include *evolutionary algorithm, parallel programming, intelligent control systems and their applications*.

 <http://orcid.org/0000-0002-3585-3332>

Muzaffer Kanaan is an associate professor of *mechatronics engineering* at Erciyes University, Turkey, where he has worked since 2009. He received his MS degree in *electrical and computer engineering* from New Jersey Institute of Technology in 1996 and PhD degrees in *electrical and computer engineering* from Worcester Polytechnic Institute in 2008. Between 1997-2008, he worked as a Distinguished Member of the Technical Staff at Verizon Laboratories in Waltham, MA, where he was responsible for various research and development projects related to *wireless and fiber-optic communication*. He has 5 U.S. Patents granted, with another two pending. His major research interests include *communication and control engineering, wireless communication, with a particular focus on the application of wireless technology in medicine*.

 <http://orcid.org/0000-0003-4510-8392>

